Malaysian Journal of Chemical Engineering & Technology 6(2) (2023) 98–106

Malaysian Journal of Chemical Engineering & Technology

Journal Homepage: http://myjms.mohe.gov.my/index.php/mjcet

e-ISSN: 2682-8588

Effect of doping on the structural properties of ZnO nanowires synthesised by ultrasonic-assisted immersion technique

[a,b] Mohamad Dzulfiqar Bakri, [a,b] Mohd Firdaus Malek*, [a,b,c] Maryam Mohammad, [a,b] Ruziana Mohamed, [a,b] Rosdiyana Hisam, [c] Mohd Hanapiah Abdullah, [a,b] Mohd Husairi Fadzilah Suhaimi, [d] Tetsuo Soga, [a,e] Mohamad Rusop Mahmood

[a]NANO-SciTech Lab (NST), Centre for Functional Materials and Nanotechnology (CFMN), Institute of Science (IOS), Universiti Teknologi MARA (UiTM), 40450 Shah Alam, Selangor, Malaysia

[b]Faculty of Applied Sciences, Universiti Teknologi MARA (UiTM), 40450 Shah Alam, Selangor, Malaysia

[c]Center for Electrical Engineering Studies, Universiti Teknologi MARA, Cawangan Pulau Pinang, 13500 Permatang Pauh, Pulau Pinang, Malaysia

[d]Department of Electrical and Mechanical Engineering, Nagoya Institute of Technology (NITech), Showa-ku, Gokiso-cho, Nagoya, 466-8555, Japan

[e]NANO-ElecTronic Centre (NET), Faculty of Electrical Engineering, Universiti Teknologi MARA (UiTM), 40450 Shah Alam, Selangor, Malaysia

*Corresponding email: mfmalek07@uitm.edu.my

Abstract

Various procedures for producing high-quality zinc oxide (ZnO) nanowires (ZnO NWs) have been developed. Nevertheless, most of it rely on harsh circumstances such as high temperature, high pressure, costly materials, and complicated procedures. As a result, this study introduces an alternative ultrasonic-assisted immersion technique due to its many advantages such as low cost, ease of handling, and low energy consumption, as well as studying the effect of different precursors on the morphological, structural, and optical properties of the ZnO NWs, thus supporting and consolidating previous discoveries and providing a clearer understanding of the mechanism of ZnO formation. The most promising desirable features have been demonstrated for chromium doped ZnO NWs. Field emission scanning electron microscopy (FESEM) was used to examine the surface morphology of the samples, and x-ray diffraction (XRD) and UV-visible (UV-Vis) were utilised to investigate the structural and optical characteristics of the ZnO NWs. It was discovered that inserting Cr as a dopant for ZnO enhanced ZnO NWs by preventing quick electron-hole recombination, revealing it as the best dopant. This id due to reduced band gap (3.231 eV), relax strain (−0.2383%) and stress (0.560 GPa), and near zero porosities.

Article Info

https://doi.org/10.24191/mjcet.v6i2.21828

Article history:

Received date: 15 March 2023
Accepted date: 24 July 2023
Published date: 31 October 2023

Keywords:

Zinc oxide
Nanomaterials
Nanowires
Immersion technique
Dopants

1.0 Introduction

Zinc oxide is one of the many nanostructured materials commonly used in the study and development of oxide-based multifunctional materials and one-dimensional nanostructures due to its unique properties, one of which is that it improves performance when applied to electrical devices such as sensors, converters, energy generators, and many more (Ding et al., 2018). Using solution synthesis techniques, a broad variety of 1-D nanometre to micrometre ZnO nanostructures (ZnO NSs) have been created, including rods, plates, tubes, rings, tetrapod, prisms, pyramids, spheres, hollow structures, flowerlike, and multi-needle shaped crystals (Alenezi, 2018; Choi & Chang, 2018; Jayaprakash et al., 2020; Jiao et al., 2019; Latif et al., 2019; Nasiri Khalil Abad et al., 2019; Nevárez Martínez et al., 2020; Saleh, 2019; Tu et al., 2018; Xu et al., 2021). Nonetheless, ZnO nanowires (ZnO NWs) were particularly notable among other nanostructures due to their quasi one-dimensional (1-D) architectures displaying quantum confinement phenomena and huge surface to volume

ratios. It can be thought of as a 1-D channel with electron, hole, and photon absorption, emission, and transport, resulting in strong confinement effects on the carriers and photons, resulting in various new optical and electrical properties for device applications such as short wavelength light emitting diodes (LEDs) and nanometre lasers (Mohammed, 2019).

Numerous methods have been established to synthesise high quality ZnO NSs. When compared to nanoparticles (NPs) deposited on a flat surface, one-dimensional nanostructures (NSs), such as nanowires grown on a substrate, offer a higher surface-to-volume ratio, and thus a higher photocatalytic activity via enhanced adsorption of target organic molecules onto the catalyst surface (Jiao et al., 2019). Other benefits include a wide range of substrate materials and geometries, as well as a simple crystal-growth method that enables much cheaper production costs than other semiconductors utilised in nanotechnology (Baruah et al., 2008; Zhou et al., 2017). Though the current growth methods for ZnO NSs, such as vapour liquid solid (VLS) growth (Kennedy et al., n.d.), chemical vapour deposition (CVD) (Bhutto et al., 2019), physical vapour deposition (PVD) (Sinju et al., 2020), and pulsed laser deposition (PLD) (Susner et al., 2014), are successful, the only drawback is that they require harsh conditions such as high temperature, high pressure, expensive materials, and complex procedures (Elzein et al., 2020). Alternatively, immersion techniques have been proposed because to their numerous benefits, including low cost, simplicity of handling, low energy usage, and scalability (Abdullah et al., 2019; Musa et al., 2020).

Another important element influencing the circumstances for the synthesis of ZnO NSs would be the dopants supplied to the precursor solution. Previous research revealed that controlled synthesis of materials at the micro- and nanoscale has been of research interest, even though it has been fraught with difficulties, because the physical and chemical properties and functionalities of a specific material are determined by its structure and/or morphology. Doping with different metal ions, particularly rare earth metals, can alter the magnetic, sensing, morphological, electrical, and optical characteristics of the host material (Zheng et al., 2022). For example, the primary purpose of the aluminium dopant was to improve electrical conductivity by substituting Zn^{2+} with Al^{3+}, which resulted in an increase in free carrier concentration. (Shah et al., 2019). Cobalt doped photocatalytic activity was increased by providing an appropriate band gap (Poornaprakash et al., 2020). Because of their significant UV absorption and near closeness of ionic radius to Zn, chromium doped materials were investigated in this study (Chinnasamy & Balasubramanian, 2020). Iron doped is a high-solubility substitutional cation in ZnO, and Fe-doped ZnO displayed p-type conductivity (Li et al., 2019). Finally, magnesium doped in this system provides a controlled band gap, minimal lattice misfit with ZnO, and excellent crystallinity (Jaballah et al., 2020).

Furthermore, because of its weak optical and electrical properties, pure ZnO cannot be employed directly in optoelectronics applications. Many studies have found that doping ZnO has a significant impact on its optical and electrical characteristics (Lehru et al., 2021; Poul Raj et al., 2020; Zhang et al., 2022). To address this issue, a good doping technique is required to enhance the optical and electrical characteristics of ZnO (Lv et al., 2018; Zhao et al., 2021). Moreover, the traditional method of producing ZnO by solution-based approach focuses on the effects of stabiliser rather than the reactant dispersion, which causes non-homogeneous reaction during the mixing process of precursor and solvent, which contributes to the formation of large particles and reduces the surface area of the nanostructures. This process will contribute to limited electron transport and excessive recombination via defects such grain boundaries (Abdel Messih et al., 2019).

In this connection, the paper is mainly focused on the study the introducing of various dopants into the intrinsic ZnO by our own modified innovative Ultrasonic-Assisted Immersion Technique. We can achieve a more homogeneous reaction process, as well as greater overall control over the nanostructure's development process.

2.0 Methodology

2.1 Material

Zinc acetate dehydrate [$(Zn(CH_3COO)_2 \cdot 2H_2O$] (99% purity), 2-methoxyethanol [$C_3H_8O_2$], zinc nitrate hexahydrate [$Zn(NO_3) \cdot 6H_2O$], hexamethylenetetramine (HMTA), [$C_6H_{12}N_4$], aluminium nitrate nonahydrate [$Al(NO_3)_3 \cdot 9H_2O$] (99% purity), cobalt(II) nitrate hexahydrate [$Co(NO_3)_2 \cdot 6H_2O$] (99% purity), chromium(III) nitrate nonahydrate [$Cr(NO_3)_3 \cdot 9H_2O$] (99% purity), iron(III) nitrate nonahydrate [$Fe(NO_3)_3 \cdot 9H_2O$] (99% purity),

and magnesium nitrate hexahydrate [$Mg(NO_3)_2 \cdot 6H_2O$] (99% purity) and deionized water. All chemicals used in this work were bought from Sigma-Aldrich company.

2.2 Preparation of ZnO nanoparticles seeded layer thin films.

Based on Zinc Oxide Nanoparticles was produced as seed layer thin films on a glass substrate using an improved ultrasonic-assisted sol-gel spin-coating process (Mamat et al., 2011, 2014). The sonicated sol-gel ZnO was made by dissolving zinc acetate dehydrate [$(Zn(CH_3COO) \cdot 2H_2O$] in 2-methoxyethanol [$C_3H_8O_2$] at ambient temperature. Then, as a stabiliser, monoethanolamine [MEA, C_2H_7NO] and a catalyst, aluminium nitrate nonahydrate [$Al(NO_3)_3 \cdot 9H_2O$] was added. The molar ratio of MEA to zinc acetate dehydrate was kept constant at 1:1, and the zinc acetate dehydrate concentration was 0.4 mol/L while the catalyst is 1% of the precursor molarity. The resulting solution was agitated for 30 minutes at 80 °C to produce a clear and homogenous solution. The solution will then be utilised to coat the glass substrate using the spin coating process, which involves depositing 10 droplets of solution onto the substrate at a speed of 3000 rpm for 30 seconds. Finally, the samples were warmed for 10 minutes in an ambient environment at 300 °C to eliminate the solvent. The deposition steps were repeated up to 5 times. Lastly the samples were annealed in a furnace at 500 °C for 1 hour.

2.3 Deposition of ZnO nanostructures via ultrasonic-assisted immersion technique

Ultrasonic-Assisted Immersion Technique was used to generate ZnO NWs. The first stage was to use our innovative optimised sonochemical approached to produce ZnO in a 37.5 mM aqueous solution generated with zinc nitrate hexahydrate [$Zn(NO_3)2H_2O$] as a precursor and hexamethylenetetramine [HMTA, $C_6H_{12}N_4$] as a stabiliser (Sofea et al., 2020). aluminium, cobalt, chromium, iron, and magnesium was added to their respective solution at 1% of the solution molarity. The reagents were dissolved and interacted for 30 minutes in a beaker with 1000 mL of distilled water as a solvent to obtain a clear and homogeneous solution. The solution was then sonicated for 30 minutes in an ultrasonic water bath at 50 °C (Hwasin Technology Powersonic 405, 40 kHz) to supple energy to the solution to archive homogeneous structure. The solution was transfer into a Scott bottle with a volume capacity of 130 ml, and the optimum seed layer-coated glass substrates were placed at the bottom. After that, the container was placed into a water bath set to 95 °C for 3 hours. After both samples were cleaned and annealed at 500 °C for 1 hour.

3.0 Results and discussion

3.1 XRD analysis

Fig. 1 depicts the XRD patterns of doped-ZnO NWs arrays thin sheets. All the diffraction peaks are consistent with a hexagonal wurtzite ZnO structure (JCPDS No. 00-036-1451). There are a series of diffraction peaks at 2=31.8°, 34.4°, 36.1°, 47.5°, 56.6°, 62.9°, and 68.0°, which correspond to the (100), (002), (101), (102), (110), (103), and (112) ZnO crystallographic planes. The strength of the diffraction peak corresponding to the (002) plane centerer at 34.4o increases significantly for all doped-ZnO NWs thin films when compared to other peaks. The (002) reflection has sharpened significantly, indicating that the c-axis of the majority of the ZnO nanocrystals is preferentially orientated perpendicular to the substrate as a result of a surface-energy-driven self-texturing mechanism (Azulay et al., 2020). Highest (002) diffraction peak is obtained when doped with chromium. The differences in the XRD pattern of the ZnO (002) peak may be explained by the ionic radii of Al^{3+} (0.53 Å), Co^{2+} (0.72 Å), Cr^{3+} (0.63 Å), Fe^{3+} (0.64 Å), and Mg^{2+} (0.72 Å), which are lower or almost comparable to that of Zn^{2+} (0.74 Å) (Huang et al., 2022; Kabbur et al., 2021; Lu et al., 2016; Qiang et al., 2022; Sharma et al., 2019; Tang et al., 2019).

Table 1 shows the relative peak intensity (RPI) of (002) orientation for ZnO NWs measured from their XRD pattern. The relative peak intensity of the (002) plane for cobalt-doped ZnO NWs is 0.4520, which is

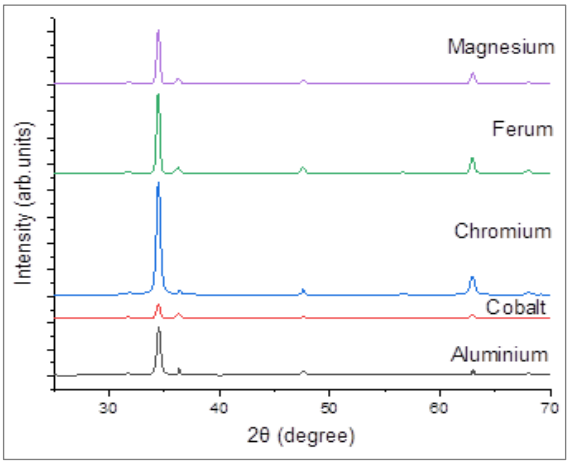

Fig. 1: The XRD patterns of ZnO NWs arrays immersed with different types of dopants

substantially higher than for magnesium-doped (0.6348), aluminium-doped (0.6432), iron-doped (0.7042), and chromium-doped (0.7599). Scherrer's equation was used to compute the average crystallite size, D, of ZnO NWs generated at various doped-ZnO NWs (Okeke et al., 2021; Sathya & Pushpanathan, 2018). The FWHM values of the ZnO NWs (002) peak were affected by the type of dopants used. Doped-ZnO NWs had typical crystallite sizes ranging from 21 to 24 nm. The calculated RPI to the doped-ZnO NWs (002) plane, FWHM, and average crystallite size of the doped-ZnO NWs are summarised in Table 1.

Different types of dopants, on the other hand, had an influence on the XRD pattern's 2θ values of ZnO (002) peak placement. The 2θ values for the samples doped with aluminium, cobalt, chromium, iron, and magnesium are 34.49°, 34.45°, 34.47°, 34.47°, and 34.47°, respectively, indicating c-axis lattice variation.

Table 2 depicts the difference in two values of doped-ZnO NW with various impurities, indicating lattice expansion/compression due to stress fluctuations (Terasako et al., 2019). The observed nature might be explained by the dopant agent's ionic radius fluctuation (Kaphle et al., 2018). The c-axis lattice of the doped ZnO NW was calculated using Bragg's law (Kasapoğlu et al., 2021). The expected lattice constants for c-films doped with aluminium, cobalt, chromium, iron, and magnesium were 5.195, 5.201, 5.198, 5.198, and 5.198 nm, respectively, according to our observations. The c-film discrepancies were unmistakable, meaning that the incorporated dopants occupied specific lattice locations, resulting in inhomogeneous unit cell deformation along the c-axis direction. As a result of the dopant inclusion, the ZnO lattice deformed significantly, changing the lattice structure and/or crystallinity of the ZnO NWs. The lattice constant 'c' of nanowires is clearly smaller than that of bulk ZnO, meaning that all samples' tensile strain and compressive stress are released (Mosalagae et al., 2020). The shift in the lattice constant implies that the strain/stress inside the nanowire structure has changed.

Normally, the strain in the films is inherent, whereas the stress inside the structure is mostly induced by the growing process (Zauner et al., 2022). The stress, film of the doped-ZnO NWs was estimated to examine the influence of different impurities on the crystal lattice and structural properties. Because of changes in atomic radii, the strain/stress of the synthesised doped-ZnO NWs varied, which also led to the shift in the (002) diffraction peak position. Smaller atomic radii and a shift in the (002) peak location's 2θ angle towards the bulk value indicate that crystal growth is slowing. This relaxation might be attributed to the incorporation of impurities into the ZnO lattice, resulting in decreased lattice compression (Belkhaoui et al., 2019). Extrinsic stress caused by lattice mismatch and the thermal expansion coefficient between samples and substrate will not be present in the nanowires structure, and the total projected stress values appear to be largely intrinsic, as evidenced by the calculated stress values. Table 2 summarises the lattice parameters, 2θ position of (002) peak, interplane distance, strain, and stress of ZnO NWs growth with various type of dopants.

3.2 FESEM images

Fig. 2 (a–e) (i) shows the surface morphology FESEM images of (a) aluminium-doped, (b) cobalt-doped, (c) chromium-doped, (d) iron-doped, and (e) magnesium-doped ZnO NWs. The hexagonal nanowires were all formed perpendicularly on the ZAO seed layers. The nanowires all had a significant (002) peak, suggesting that they grew along the c-axis. The

Table 1: The variation of the structural parameters of ZnO NWs doped with various types of dopants

Dopants	RPI (002)	FWHM (Degree)	Crystallite size (nm)
Al	0.6432	0.4040	21.49
Co	0.4520	0.4390	19.77
Cr	0.7599	0.4337	20.01
Fe	0.7042	0.3591	24.17
Mg	0.6348	0.3658	23.73

Table 2: Lattice parameters, 2θ position of (002) peak, interplane distance, strain and stress of ZnO NWs immersed with various type of dopants

Dopants	Lattice parameters c-film (Å)	2θ of (002) peak (Degree)	Interplane distance, d (Å)	Strain of c-axis (%)	Stress (GPa)
Al	5.195	34.49	2.597	-0.2944	0.685
Co	5.201	34.45	2.600	-0.1821	0.424
Cr	5.198	34.47	2.599	-0.2383	0.560
Fe	5.198	34.47	2.599	-0.2383	0.560
Mg	5.198	34.47	2.599	-0.2383	0.560

average diameters of aluminium-doped, cobalt-doped, chromium-doped, iron-doped, and magnesium-doped ZnO NWs were 55.92, 123.08, 79.00, 36.29, and 127.10 nm, respectively. Changes in the atomic radii of Zn and the dopants are hypothesised to produce the fluctuation in the diameter of the nanowires. During the deposition process, different dopants may estimate the diameter size of the nanowires, where the doping process may occur via interstitial and/or substitution reaction. Fig. 2 (a–e) (ii) shows the length of the doped-ZnO NWs in cross section. The length of each sample was determined using a cross-sectional view of the FESEM images. aluminium-doped, cobalt-doped, chromium-doped, iron-doped, and magnesium-doped ZnO NWs had lengths of 468.90, 680.90, 729.60, 922.2, and 736.7 nm, respectively. The aspect ratio of the nanowires found to be varied with different dopant introduced with chromium-doped ZnO NWs have highest aspect ratio of 22.8 (Kim et al., 2018). Table 3 summarises the average values of the diameter, length, and aspect ratio of ZnO NWs doped with various types of dopants. The FESEM images clearly illustrate that different types of dopants influence the morphologies of the nanowire formations.

3.3 UV-vis analysis

Fig. 3 displays the optical transmittance spectra of aluminium-doped, cobalt-doped, chromium-doped, iron-doped, and magnesium-doped ZnO NWs from 350 to 800 nm. All the nanowires showed a greater transmission characteristic of more than 72% in the visible light domain, which is consistent with the structure's previous measured length. According to the data analysis, the cobalt-doped ZnO NWs showed the highest average transmittance in the visible region (87.15%). On the other hand, the chromium-doped ZnO NWs at the same wavelength showed the lowest transmittance of 72.08%. This corresponds to the XRD peak intensity pattern.

Fig. 3 displays the optical absorption coefficient spectra of aluminium-doped, cobalt-doped, chromium-doped, iron-doped, and magnesium-doped ZnO NWs between 350 and 800 nm. The variation in absorption edges is visible, which might be due to the difference in ionic radius between the impurity ions that cause light scattering effects in nanowire formation (Mohamed & Ismail, 2021).

Table 3: Average diameter, length and aspect ratio of ZnO NWs immersed with various types of dopants

Dopants	Average Diameter (nm)	Length (µm)	Aspect ratio
Al	55.92	0.469	8.39
Co	123.01	0.611	4.97
Cr	79.00	0.730	10.3
Fe	36.288	0.816	22.8
Mg	124.10	0.615	4.96

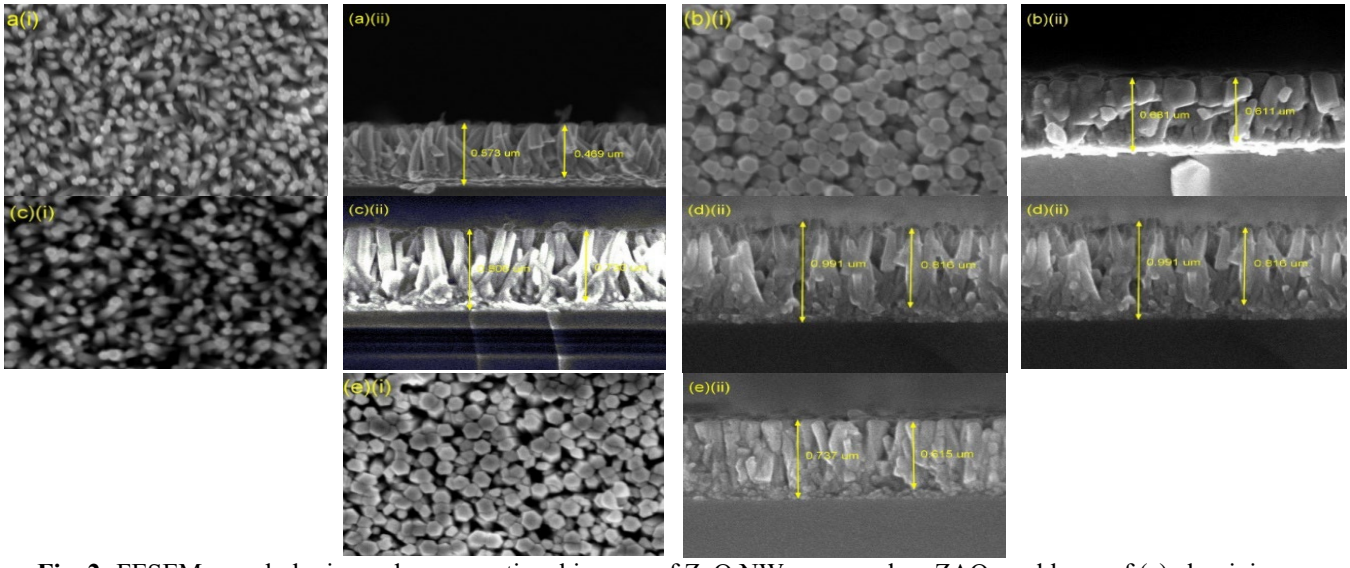

Fig. 2: FESEM morphologies and cross-sectional images of ZnO NWs prepared on ZAO seed layer of (a) aluminium-doped, (b) cobalt-doped, (c) chromium-doped, (d) iron-doped and (e) magnesium-doped ZnO NWs

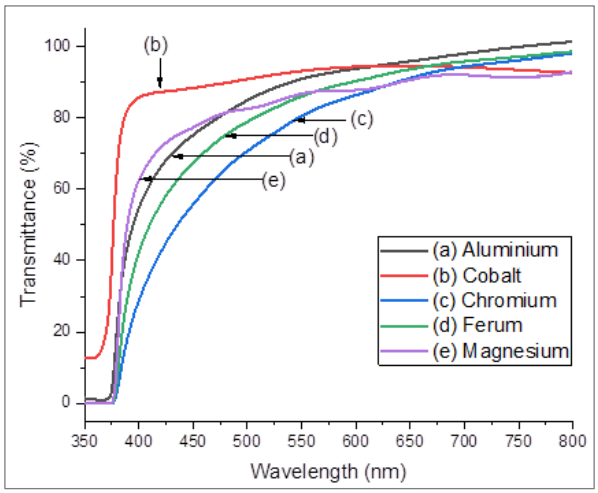

Fig. 3: transmittance spectra of (a) aluminium-doped, (b) cobalt-doped, (c) chromium-doped, (d) iron-doped, and (e) magnesium-doped ZnO NWs

4.0 Conclusions

It can be concluded that thin films of vertically aligned ZnO NWs arrays were successfully produced using different dopants. ZnO NWs arrays with dopants aluminium, cobalt, chromium, iron, and magnesium had average diameters of 55.9, 123.01, 79.00, 36.29, and 124.10 nm, respectively. According to cross-sectional pictures, the thickness of the samples was 0.469, 0.611, 0.730, 0.816, and 0.615 nm for Al, Co, Cr, Fe, and Mg, respectively. All the nanowire samples have a polycrystalline hexagonal wurtzite structure dominated by the (002) peak, showing that growth is along the c-axis orientation. The Chromium-ZnO NWs displayed the long structure and the most significant (002) peak in all the samples' XRD patterns. The highest peak intensity of c-film nanowires, the high aspect ratio of nanowires is all found in chromium-ZnO NWs. All the findings highlight to the importance of controlling vertically oriented ZnO NWs thin films. This is done to enhance film surface area and uniformity of doping element distribution.

Contribution statement

Mohd Firdaus Malek, Tetsuo Soga & Mohamad Rusop Mahmood: Conceptualisation and supervision; **Mohd Firdaus Malek, Maryam Mohammad & Ruziana Mohamed:** Methodology; **Dzulfiqar Bakri & Mohd Firdaus Malek:** Formal analysis and investigation; **Mohd Firdaus Malek, Tetsuo Soga & Mohamad Rusop Mahmood:** Resources; **Dzulfiqar Bakri & Mohd Firdaus Malek:** Writing-original draft; **Rosdiyana Hisam, Mohd Hanapiah Abdullah, & Mohd Husairi Fadzilah Suhaimi:** Writing-review and editing; **Mohd Firdaus Malek & Mohamad Rusop Mahmood:** Project administration.

Conflict of Interest

The authors declare that they have no known competing financial interests or personal relationships that could have appeared to influence the work reported in this paper.

Acknowledgement

This work was supported by Grant No. 600-RMC/SRC/5/3 (027/2020) under the Ministry of Education (MOHE) and the Universiti Teknologi MARA (UiTM), Malaysia. The authors would like to thank the Research Management Centre (RMC), Universiti Teknologi MARA (UiTM), Malaysia, for their support. The authors would also like to thank Mr. Salifairus Mohammad Jafar (UiTM Senior Science Officer) and Mr. Mohd Azlan Jaafar (UiTM Assistant Engineer) for their kind support to this research.

References

Abdel Messih, M. F., Ahmed, M. A., Soltan, A., & Anis, S. S. (2019). Synthesis and characterization of novel Ag/ZnO nanoparticles for photocatalytic degradation of methylene blue under UV and solar irradiation. *Journal of Physics and Chemistry of Solids*, *135*, 109086. https://doi.org/10.1016/j.jpcs.2019.109086

Abdullah, M. A. R., Mamat, M. H., Ismail, A. S., Malek, M. F., Suriani, A. B., Ahmad, M. K., Shameem Banu, I. B., Amiruddin, R., & Rusop, M. (2019). Direct and seedless growth of Nickel Oxide nanosheet architectures on ITO using a novel solution immersion method. *Materials Letters*, *236*, 460–464. https://doi.org/10.1016/j.matlet.2018.10.163

Alenezi, M. R. (2018). Hierarchical zinc oxide nanorings with superior sensing properties. *Materials Science and Engineering B: Solid-State Materials for Advanced Technology*, *236–237*(January), 132–138. https://doi.org/10.1016/j.mseb.2018.11.011

Azulay, A. R., Turkulets, Y., Gaudio, D. Del, Goldman, R. S., & Shalish, I. (2020). Why do nanowires grow with their c-axis vertically-aligned in the absence of epitaxy? *Scientific Reports*, *10*(1), 1–6. https://doi.org/10.1038/s41598-020-63500-y

Baruah, S., Rafique, F. F., & Dutta, J. (2008). Visible light photocatalysis by tailoring crystal defections in zinc oxide nanostructures. *Nano*, *3*(5), 399–407. https://doi.org/10.1142/S179329200800126X

Belkhaoui, C., Mzabi, N., & Smaoui, H. (2019). Investigations on structural, optical and dielectric properties of Mn doped ZnO nanoparticles synthesized by co-precipitation method. *Materials Research Bulletin*, *111*, 70–79. https://doi.org/10.1016/j.materresbull.2018.11.006

Bhutto, W. A., Soomro, A. M., Nizamani, A. H., Saleem, H., Khaskheli, M. A., Sahito, A. G., Das, R., Khan, U. A., & Saleem, S. (2019). Controlled Growth of Zinc Oxide Nanowire Arrays by Chemical Vapor Deposition (CVD) Method. *International Journal of Computer Science and Network Security*, *19*(8), 135–141.

Chinnasamy, M., & Balasubramanian, K. (2020). Enhanced UV photodetection behavior of Cr doped wurtzite ZnO crystalline nanorods. *Optical Materials*, *110*(October), 110492. https://doi.org/10.1016/j.optmat.2020.110492

Choi, K. S., & Chang, S. P. (2018). Effect of structure morphologies on hydrogen gas sensing by ZnO nanotubes. *Materials Letters*, *230*(July), 48–52. https://doi.org/10.1016/j.matlet.2018.07.031

Ding, M., Guo, Z., Zhou, L., Fang, X., Zhang, L., Zeng, L., Xie, L., & Zhao, H. (2018). One-dimensional zinc oxide nanomaterials for application in high-performance advanced optoelectronic devices. *Crystals*, *8*(5), 1–29. https://doi.org/10.3390/cryst8050223

Elzein, B., Yao, Y., Barham, A. S., Dogheche, E., & Jabbour, G. E. (2020). Toward the growth of self-catalyzed zno nanowires perpendicular to the surface of silicon and glass substrates, by pulsed laser deposition. *Materials*, *13*(19), 1–14.

Huang, H., Xia, X., Yun, J., Huang, C., Li, D., Chen, B., Yang, Z., & Zhang, W. (2022). Interfacial engineering of hydrated vanadate to promote the fast and highly reversible H+/Zn2+ co-insertion processes for high-performance aqueous rechargeable batteries. *Energy Storage Materials*, *52*(August), 473–484. https://doi.org/10.1016/j.ensm.2022.08.016

Jaballah, S., Benamara, M., Dahman, H., Ly, A., Lahem, D., Debliquy, M., & Mir, L. El. (2020). Effect of Mg-doping ZnO nanoparticles on detection of low ethanol concentrations. *Materials Chemistry and Physics*, *255*. https://doi.org/10.1016/j.matchemphys.2020.123643

Jayaprakash, N., Suresh, R., Rajalakshmi, S., Raja, S., Sundaravadivel, E., Gayathri, M., & Sridharan, M. (2020). One-step synthesis, characterisation, photocatalytic and bio-medical applications of ZnO nanoplates. *Materials Technology*, *35*(2), 112–124. https://doi.org/10.1080/10667857.2019.1659533

Jiao, T., Kutsanedzie, F. Y. H., Xu, J., Viswadevarayalu, A., Hassan, M. M., Li, H., Xu, Y., & Chen, Q. (2019). SERS-signal optimised AgNPs-plated-ZnO nanoflower-like structure synthesised for sensing applications. *Physics Letters, Section A: General, Atomic and Solid State Physics*, *383*(12), 1312–1317. https://doi.org/10.1016/j.physleta.2019.01.026

Kabbur, S. M., Nadargi, D. Y., Kambale, R. C., Ghodake, U. R., & Suryavanshi, S. S. (2021). Microstructure and magnetic interactions of Co2+ substituted NiCuZn ferrites. *Journal of Magnetism and Magnetic Materials*, *517*(August 2020), 167376. https://doi.org/10.1016/j.jmmm.2020.167376

Kaphle, A., Borunda, M. F., & Hari, P. (2018). Influence of cobalt doping on residual stress in ZnO nanorods. *Materials Science in Semiconductor Processing*, *84*(March), 131–137. https://doi.org/10.1016/j.mssp.2018.05.019

Kasapoğlu, A. E., Habashyani, S., Baltakesmez, A., İskenderoğlu, D., & Gür, E. (2021). The effect of the change in the amount of Sb doping in ZnO nanorods for hydrogen gas sensors. *International Journal of Hydrogen Energy*, *46*(41), 21715–21725. https://doi.org/10.1016/j.ijhydene.2021.03.229

Kennedy, O. W., White, E. R., Shaffer, M. S. P., & Warburton, P. A. (n.d.). *Vapour-liquid-solid growth of ZnO-ZnMgO core – shell nanowires by gold-catalysed molecular beam epitaxy*. 2–7.

Kim, M. J., Alvarez, S., Yan, T., Tadepalli, V., Fichthorn, K. A., & Wiley, B. J. (2018). Modulating the Growth Rate, Aspect Ratio, and Yield of Copper Nanowires with Alkylamines. *Chemistry of Materials*, *30*(8), 2809–2818. https://doi.org/10.1021/acs.chemmater.8b00760

Latif, M. M. A. El, Ibrahim, A. M., & Gohr, M. S. (2019). *Alcohol / water mediated preparation of ZnO nano hollow sphere*. *September*.

Lehru, R., Radhanpura, J., Kumar, R., Zala, D., Vadgama, V. S., Dadhich, H., Rathod, V. R., Trivedi, R. K., Pandya, D. D., Shah, N. A., & Solanki, P. S. (2021). Studies on electrical properties of Fe doped ZnO nanostructured oxides synthesized by sol–gel method. *Solid State Communications*, *336*(December 2020), 114415. https://doi.org/10.1016/j.ssc.2021.114415

Li, H., Zhao, W., Liu, Y., Liang, Y., Ma, L., Zhu, M., Yi, C., Xiong, L., & Gao, Y. (2019). High-level-Fe-doped P-type ZnO nanowire array/n-GaN film for ultraviolet-free white light-emitting diodes. *Materials Letters*, *239*, 45–47. https://doi.org/10.1016/j.matlet.2018.12.041

Lu, M., Han, E., Zhu, L., Chen, S., & Zhang, G. (2016). The effects of Ti4 +-Fe3 + co-doping on Li[Ni1/3Co1/3Mn1/3]O2. *Solid State Ionics*, *298*, 9–14. https://doi.org/10.1016/j.ssi.2016.10.014

Lv, Y., Zhang, Z., Yan, J., Zhao, W., & Zhai, C. (2018). Al doping influences on fabricating ZnO nanowire arrays: Enhanced field emission property. *Ceramics International*, *44*(7), 7454–7460. https://doi.org/10.1016/j.ceramint.2018.01.118

Mamat, M. H., Khusaimi, Z., Musa, M. Z., Malek, M. F., & Rusop, M. (2011). Fabrication of ultraviolet photoconductive sensor using a novel aluminium-doped zinc oxide nanorod-nanoflake network thin film prepared via ultrasonic-assisted sol-gel and immersion methods. *Sensors and Actuators, A: Physical*, *171*(2), 241–247. https://doi.org/10.1016/j.sna.2011.07.002

Mamat, M. H., Malek, M. F., Hafizah, N. N., Khusaimi, Z., Musa, M. Z., & Rusop, M. (2014). Sensors and Actuators B : Chemical Fabrication of an ultraviolet photoconductive sensor using novel nanostructured , nanohole-enhanced , aligned aluminium-doped zinc oxide nanorod arrays at low immersion times. *Sensors & Actuators: B. Chemical*, *195*, 609–622. https://doi.org/10.1016/j.snb.2014.01.082

Mohamed, R. M., & Ismail, A. A. (2021). Mesoporous α-Fe2O3/ZnO heterojunction with a synergistic effect forrapid and efficient reduction of mercury ions. *Separation and Purification Technology*, *266*(November 2020), 118360. https://doi.org/10.1016/j.seppur.2021.118360

Mohammed, D. S. (2019). *High Quality Factor Plasmonic Laser Based on Two Cavity Design*. *August*.

Mosalagae, K., Murape, D. M., & Lepodise, L. M. (2020). Effects of growth conditions on properties of CBD synthesized ZnO nanorods grown on ultrasonic spray pyrolysis deposited ZnO seed layers. *Heliyon*, *6*(7), e04458. https://doi.org/10.1016/j.heliyon.2020.e04458

Musa, M. Z., Mamat, M. H., Vasimalai, N., Shameem Banu, I. B., Malek, M. F., Ahmad, M. K., Suriani, A. B., Mohamed, A., & Rusop, M. (2020). Fabrication and structural properties of flower-like TiO2 nanorod array films grown on glass substrate without FTO layer. *Materials Letters*, *273*, 127902. https://doi.org/10.1016/j.matlet.2020.127902

Nasiri Khalil Abad, S., Moghaddam, J., Mozammel, M., Mostafaei, A., & Chmielus, M. (2019). Growth mechanism and charge transport properties of hybrid Au/ZnO nanoprisms. *Journal of Alloys and Compounds*, *777*, 1386–1395. https://doi.org/10.1016/j.jallcom.2018.11.084

Nevárez Martínez, M. C., Bajorowicz, B., Klimczuk, T., Żak, A., Łuczak, J., Lisowski, W., & Zaleska-Medynska, A. (2020). Synergy between AgInS2 quantum dots and ZnO nanopyramids for photocatalytic hydrogen evolution and phenol degradation. *Journal of Hazardous Materials*, *398*(June). https://doi.org/10.1016/j.jhazmat.2020.123250

Okeke, I. S., Agwu, K. K., Ubachukwu, A. A., Madiba, I. G., Maaza, M., Whyte, G. M., & Ezema, F. I. (2021). Impact of particle size and surface defects on antibacterial and photocatalytic activities of undoped and Mg-doped ZnO nanoparticles, biosynthesized using one-step simple process. *Vacuum*, *187*(February), 110110. https://doi.org/10.1016/j.vacuum.2021.110110

Poornaprakash, B., Chalapathi, U., Subramanyam, K., Vattikuti, S. V. P., & Park, S. H. (2020). Wurtzite phase Co-doped ZnO nanorods: Morphological, structural, optical, magnetic, and enhanced photocatalytic characteristics. *Ceramics International*, *46*(3), 2931–2939. https://doi.org/10.1016/j.ceramint.2019.09.289

Poul Raj, I. L., Valanarasu, S., Hariprasad, K., Ponraj, J. S., Chidhambaram, N., Ganesh, V., Ali, H. E., & Khairy, Y. (2020). Enhancement of optoelectronic parameters of Nd-doped ZnO nanowires for photodetector applications. *Optical Materials*, *109*(July), 110396. https://doi.org/10.1016/j.optmat.2020.110396

Qiang, M., Yin, X., Lin, H., Hong, R., Zhang, D., Zhang, Z., Zhou, S., Chen, J., Tian, Y., Zheng, G., & Ding, Y. (2022). ZnAl2O4:Cr3+ translucent ceramic phosphor with thermally stable far-red luminescence. *Optical Materials*, *133*(September), 112887. https://doi.org/10.1016/j.optmat.2022.112887

Saleh, S. M. (2019). ZnO nanospheres based simple hydrothermal route for photocatalytic degradation of azo dye. *Spectrochimica Acta - Part A: Molecular and Biomolecular Spectroscopy*, *211*, 141–147. https://doi.org/10.1016/j.saa.2018.11.065

Sathya, M., & Pushpanathan, K. (2018). Synthesis and Optical Properties of Pb Doped ZnO Nanoparticles. *Applied Surface Science*, *449*, 346–357. https://doi.org/10.1016/j.apsusc.2017.11.127

Shah, A., Ahmad, M., Rahmanuddin, Khan, S., Aziz, U., Ali, Z., Khan, A., & Mahmood, A. (2019). The role of Al doping on ZnO nanowire evolution and optical band gap tuning. *Applied Physics A: Materials Science and Processing*, *125*(10), 14–17. https://doi.org/10.1007/s00339-019-3005-y

Sharma, H. K., Archana, R., Sankar ganesh, R., Singh, B. P., Ponnusamy, S., Hayakawa, Y., Muthamizhchelvan, C., Raji, P., Kim, D. Y., & Sharma, S. K. (2019). Substitution of Al3+ to Zn2+ sites of ZnO enhanced the photocatalytic degradation of methylene blue under irradiation of visible light. *Solid State Sciences*, *94*, 45–53. https://doi.org/10.1016/j.solidstatesciences.2019.05.011

Sinju, K. R., Ramgir, N. S., Pathak, A., Debnath, A. K., & Muthe, K. P. (2020). Multiple sensor array based on ZnO nanowires for electronic nose applications towards toxic gases. *AIP Conference Proceedings*, *2265*(November). https://doi.org/10.1063/5.0017841

Sofea, Z., Malek, M. F., Mohamed, R., Mamat, M. H., & Rusop, M. (2020). *Optical and Structural Properties of Zinc Oxide : Graphene Oxide Nanorods Via Sol-Gel Assisted Immersion Technique*. *2*(October 2019), 19–24.

Susner, M. A., Carnevale, S. D., Kent, T. F., Gerber, L. M., Phillips, P. J., Sumption, M. D., & Myers, R. C. (2014). Catalyst-free ZnO nanowires on silicon by pulsed laser deposition with tunable density and aspect ratio. *Physica E: Low-Dimensional Systems and Nanostructures*, *62*, 95–103. https://doi.org/10.1016/j.physe.2014.04.023

Tang, B., Xiang, Q., Fang, Z., Zhang, X., Xiong, Z., Li, H., Yuan, C., & Zhang, S. (2019). Influence of Cr 3+ substitution for Mg 2+ on the crystal structure and microwave dielectric properties of CaMg 1-x Cr 2x/3 Si 2 O 6 ceramics. *Ceramics International*, *45*(9), 11484–11490. https://doi.org/10.1016/j.ceramint.2019.03.016

Terasako, T., Obara, S., Yagi, M., Nomoto, J., & Yamamoto, T. (2019). Structural and photoluminescence properties of ZnO nanorods grown on ion-plated Ga-doped ZnO seed layers by chemical bath deposition and fabrication of poly(3,4-ethylenedioxythiophene) poly(styrenesulfonate)/ZnO nanorods heterostructures. *Thin Solid Films*, *677*, 109–118. https://doi.org/10.1016/j.tsf.2019.03.025

Tu, Y., Chen, S., Li, X., Gorbaciova, J., Gillin, W. P., Krause, S., & Briscoe, J. (2018). Control of oxygen vacancies in ZnO nanorods by annealing and their influence on ZnO/PEDOT:PSS diode behaviour. *Journal of Materials Chemistry C*, *6*(7), 1815–1821. https://doi.org/10.1039/c7tc04284a

Xu, F., Zhou, C., & Ho, H. P. (2021). A rule for operation temperature selection of a conductometric VOC gas sensor based on ZnO nanotetrapods. *Journal of Alloys and Compounds*, *858*, 158294. https://doi.org/10.1016/j.jallcom.2020.158294

Zauner, L., Hahn, R., Aschauer, E., Wojcik, T., Davydok, A., Hunold, O., Polcik, P., & Riedl, H. (2022). Assessing the fracture and fatigue resistance of nanostructured thin films. *Acta Materialia*, *239*, 118260. https://doi.org/10.1016/j.actamat.2022.118260

Zhang, W., Li, P., Li, Y., Chen, H., Wang, X., Ma, J., & Zhao, X. (2022). Structural, optical and electrical properties of sol-gel spin-coated Ga and F Co-doped ZnO films. *Thin Solid Films*, *746*(January), 139121. https://doi.org/10.1016/j.tsf.2022.139121

Zhao, S., Shen, Y., Li, A., Chen, Y., Gao, S., Liu, W., & Wei, D. (2021). Effects of rare earth elements doping on gas sensing properties of ZnO nanowires. *Ceramics International*, *47*(17), 24218–24226. https://doi.org/10.1016/j.ceramint.2021.05.133

Zheng, B., Fan, J., Chen, B., Qin, X., Wang, J., Wang, F., Deng, R., & Liu, X. (2022). Rare-Earth Doping in Nanostructured Inorganic Materials. *Chemical Reviews*, *122*(6), 5519–5603. https://doi.org/10.1021/acs.chemrev.1c00644

Zhou, Q., Wen, J. Z., Zhao, P., & Anderson, W. A. (2017). Synthesis of vertically-aligned zinc oxide nanowires and their application as a photocatalyst. *Nanomaterials*, *7*(1), 1–13. https://doi.org/10.3390/nano7010009